Photoelectron–Auger-electron angular-momentum transfer in core-ionized Ar: Beyond the standard post-collision-interaction model

R. Guillemin,[1] L. Gerchikov,[2] S. Sheinerman,[3] M. Zmerli,[1] T. Marin,[1] L. Journel,[1] O. Travnikova,[1] T. Marchenko,[1] B. Lassalle-Kaiser,[4] M. N. Piancastelli,[1,5] and M. Simon[1]

[1]*Sorbonne Universités, CNRS, UMR 7614, Laboratoire de Chimie Physique Matière et Rayonnement, F-75005 Paris, France*
[2]*Department of Experimental Physics, Peter the Great St. Petersburg Polytechnic University, 195251 St. Petersburg, Russia*
[3]*Department of Physics, St. Petersburg State Marine Technical University, 190121 St. Petersburg, Russia*
[4]*Synchrotron SOLEIL, l'Orme des Merisiers, Saint-Aubin, BP 48, 91192 Gif-sur-Yvette Cedex, France*
[5]*Department of Physics and Astronomy, Uppsala University, P.O. Box 516, SE-751 20 Uppsala, Sweden*

(Received 5 December 2018; published 13 June 2019)

Electron-ion coincidence experimental data obtained following argon 1*s* photoionization are reported. Slow photoelectrons were measured in coincidence with Ar^+ and Ar^{2+} ions, and the β angular distribution parameter was obtained. The measured beta parameter for the Ar^{2+}-photoelectron coincidence measurements shows a significant deviation from the $\beta = 2$ expected value. With the support of a quantum mechanical theory of post-collision interaction (PCI) which goes beyond the standard model, we attribute this deviation to angular-momentum exchange due to the interaction of the photoelectron with the Auger electron, while the role of the residual ion is negligible. The main mechanism of angular-momentum transfer and its effect on the asymmetry parameter β near the photoionization threshold are considered.

DOI: 10.1103/PhysRevA.99.063409

I. INTRODUCTION

Studies of photoexcitation and photoionization of deep core levels in atoms and molecules and subsequent decay patterns have become feasible recently in the so-called tender x-ray domain (2–12 keV) under state-of-the-art experimental conditions, which has given a great impulse to investigations of the dynamics of photoemission and relaxation processes involving inner shells (see, e.g., [1–5]). An important category of phenomena, very informative about such dynamics, is post-collision interaction (PCI). Its physical description is the following: during nonradiative (Auger) decay, Coulomb interaction between the outgoing photoelectron, the Auger electron, and the atomic or molecular ion left behind manifests itself as shifts and distortions of both photoelectron and Auger spectral features. The PCI phenomenon has received considerable attention in the last several decades (for a review, see [6,7]). In the classical picture, PCI distortion of the energy distribution implies an energy exchange between the emitted Auger electron, photoelectron, and residual ion. Several recent studies have been reported about PCI peak distortion and shifts (see, e.g., [1,4,8–12]). In particular, we have investigated PCI in argon 1*s* photoelectron spectra associated with the different ionic charge states created after core excitation, by electron-ion coincidences and theoretical calculations, which has allowed us to unravel the complicated dynamics of the Auger cascade following deep core ionization, and even to estimate the lifetime of the various intermediate states [1]. While the energetics of the PCI effect is well understood, much less attention has been paid to another aspect of it, namely its possible influence on the emitted electron angular distribution. In general, one can expect that the emitted electrons can exchange not only energy but also angular momentum in the course of PCI. Such an exchange could modify the electron emission angular pattern. Considering near-threshold photoionization of a deep atomic level followed by a single Auger decay, the available standard PCI theories (see, e.g., [13–17]) predict that the energy distortion is due mainly to the interaction of the slow photoelectron with the ionic field, which changes during the emission of the fast Auger electron. The interaction between the photoelectrons and Auger electrons is neglected. Therefore, within this approach, the angular distribution of the photoelectron is determined solely by the nature of the ionized level.

For linearly polarized ionizing radiation, the differential cross section can be written as [18]

$$d\sigma/d\Omega = \sigma/(4\pi)[1 + \beta P_2(\cos\theta)], \tag{1}$$

where σ is the total cross section, P_2 is the second-order Legendre polynomial, θ is the angle between the axis of linear polarization of the incident photon and the direction of the outgoing photoelectron, and β is the asymmetry parameter. In case of photoemission from the ns^2 shell, the emitted electron can only have one value of angular momentum, $l = 1$, if the process is considered in the framework of the standard one-electron nonrelativistic approximation, and $\beta = 2$ for all energies of the emitted photoelectron [19]. Possible deviations from this value due to photoelectron–Auger-electron interaction are not considered in standard near-threshold PCI theories [13–17]. However, such an effect should in principle be present.

In this paper we report electron-ion coincidence experimental data obtained following argon 1*s* photoionization. Slow photoelectrons with kinetic energy of 2, 4, and 10 eV were measured in coincidence with Ar^+ and Ar^{2+} ions. From the detected photoelectron momentum patterns, the β angular

distribution parameter was obtained. The main result is that β is exactly equal to 2 for photoelectrons in coincidence with Ar^+, as expected for photoionization from a ns^2 shell, but it shows a very significant deviation from 2 for Ar^{2+}. The rationale is that for Ar^+ there is no Auger electron emission, and therefore no perturbation on the outgoing photoelectron. In previous publications [5,20], we have shown that Ar^{2+} is produced primarily by $K\alpha$ radiative decay followed by Auger emission, and therefore the fast Auger electron can catch up with the photoelectron and influence its angular distribution. Although highly charged ions up to Ar^{7+} are formed after 1s ionization [5], only Ar^{2+} offers the opportunity to observe the effect of PCI between one photoelectron and one Auger electron. All higher charge states involve the emission of several Auger electrons, either by cascade Auger decay or via double direct Auger decay. In the case of direct emission of two Auger electrons, the energy is shared between the two outgoing electrons, and the energy distribution has a characteristic U shape [21]. The low energy side of this distribution appears as a continuum beneath the photoelectron peak, and adds an isotropic component to the electron angular distribution. Coincidence measurements between photoelectrons and Ar^{2+} ions filters out these slow Auger electrons.

II. METHODS

A. Experiment

Our experimental approach consisted in measuring in coincidence the 1s photoelectron and the charged ion produced by the 1s hole decay. The experimental setup has already been described in detail elsewhere [22]. Briefly, the apparatus consists of a double spectrometer that combines time-of-flight (TOF) and imaging techniques for full momentum vector measurements of all charged particles detected in coincidence. The setup is represented schematically in Fig. 1. Electrons and ions are separated and accelerated in opposite directions with a static electric field towards position-sensitive detectors based on microchannel plates and delay lines. The measurement of the TOF and impact position provides the three components of the velocity vector of each detected particle. The sample gas is introduced in the interaction zone as a supersonic cooled jet to eliminate thermal contribution to the velocity vector. The supersonic jet crosses the ionizing radiation at the center of the double spectrometer. X-ray photons are produced by synchrotron radiation. The experiment was performed at beamline LUCIA of the French national synchrotron source SOLEIL, which provided x rays with 100% linear polarization during eight-bunch operation of the storage ring [23]. Highly charged ions up to Ar^{7+} are formed after 1s ionization [5]. Ionization events associated with the formation of Ar^+ or Ar^{2+} are selected by filtering all recorded events on the basis of the ion TOF. The monochromator energy was calibrated on the position of the resonant $1s \rightarrow 4p$ transition at 3203.5 eV and measurements were performed at photon energies of 2, 4, and 10 eV above the 1s ionization threshold (3206.26 eV [24]).

B. Theoretical calculations

These newly obtained experimental results are explained on the grounds of our calculations, which show a β value

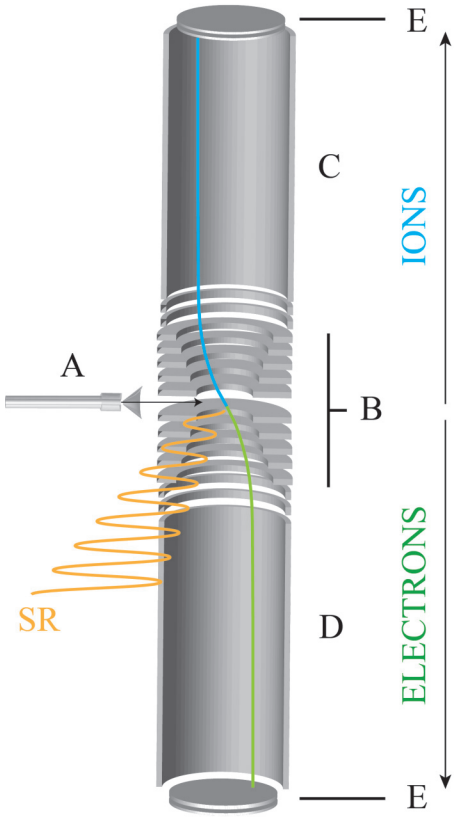

FIG. 1. Schematics of the coincidence setup: electron-ions coincidence setup. A: molecular jet; B: electrostatic lenses; C: ion time-of-flight spectrometer; D: electron time-of-flight spectrometer; E: 80 mm microchannel plates; SR: synchrotron radiation. See text for details.

significantly lower than 2 for the Ar^{2+} case. A quantum many-body theory beyond the standard near-threshold PCI approaches [13–17] has been developed by us [25,26] in order to take into account the angular-momentum exchange due to interaction of the photoelectron with both the Auger electron and the residual ion. Several mechanisms of angular-momentum exchange between the photoelectron and the residual ion, e.g., a rearrangement of the open outer shells of the ion, intershell electron correlation, and the photoelectron scattering on the anisotropic field of the residual ion—have been considered. The most effective mechanism was found to be the precession of the photoelectron angular momentum in the field of the residual ion. However, the shift of parameter β due to this mechanism is smaller by orders of magnitude than the observed β deviation. The weakness of the photoelectron-ion angular-momentum exchange is explained by the long delay between the s-shell photoionization and the Auger emission. Consequently angular-momentum transfer starts when the photoelectron is already located far away from the ion that strongly suppresses its efficiency. Thus, the interaction between photoelectrons and Auger electrons provides the main contribution for angular-momentum transfer. This is at variance with the PCI-distorted energy distribution, where for near-threshold ionization the main factor is the photoelectron-ion interaction and the role of the fast Auger electrons is negligible.

The considered photoionization processes is represented by the two-step scheme

$$\gamma + \mathrm{Ar} \to e_{ph} + \mathrm{Ar}^{+*}(1s^{-1}) \to e_{ph}(\mathbf{p}_1) + e_A(\mathbf{p}_2) + \mathrm{Ar}^{2+}(3p^{-2}). \quad (2)$$

In the first step the photoabsorption yields the metastable ion Ar^{+*} with deep $1s$ vacancy and the photoelectron e_{ph} in some intermediate state with angular momentum $l = 1$ and complex energy $\varepsilon_0 + i\Gamma/2$, where ε_0 is the excess of the photon energy above the threshold; Γ is the width of the created inner shell vacancy. The energy imaginary part originates from the inner vacancy decay. The second step of the scheme (2) represents the decay process leading to the photoelectron in the final state $e_{ph}(\mathbf{p}_1)$, Auger electron $e_A(\mathbf{p}_2)$, and the doubly charged ion Ar^{2+}.

We evaluate the angular-momentum exchange between the slow photoelectron and the fast Auger electron using the theoretical approach developed in [25]. The considered photoionization processes (2) occur via the long living intermediate state Ar^{+*}. That is why its amplitude is represented as a product of the photoabsorption amplitude M_1 and the amplitude M_2 of the Auger decay of the autoionizing state A^{+*} and subsequent PCI processes [16]:

$$\mathcal{A} = M_1 \langle \Psi_{\mathbf{p}_1,\mathbf{p}_2}\, \Phi_{A^{2+}} | \hat{M}_2 | \Psi_{\varepsilon_0 + i\Gamma/2} \Phi_{A^{+*}} \rangle. \quad (3)$$

Here the operator of the Auger decay is denoted by $\hat{M}_2$, $\Phi_{A^{+*}}$ denotes the wave function of A^{+*}, $\Psi_{\varepsilon_0+i\Gamma/2}$ is the wave function of a photoelectron e_{ph} with complex energy $\varepsilon_0 + i\Gamma/2$ moving in the field of the singly charged ion, vectors $\mathbf{p}_{1,2}$ stand for the momenta of photoelectron $e_{ph}(\mathbf{p}_1)$ and Auger electron $e_A(\mathbf{p}_2)$ respectively, and A^{2+} is final state of the doubly charged residual ion.

The final state of the emitted electrons e_{ph}, e_A, and the residual ion A^{2+} is described by the correlated many-body wave function, taking into account the conservation of the total angular momentum. However, as demonstrated in Ref. [25], these correlations have a minor effect on the angular-momentum transfer. It is quite natural because of the long delay $\tau = 1/\Gamma \gg 1$ between the photoionization and the Auger ionization that ensures that PCI takes place far from the target atom. At such large distances influence of electron correlations between the emitted electrons and the atomic electrons on angular-momentum transfer is strongly suppressed. This fact allows us to write the final wave function in the PCI amplitude $\mathcal{A}$ (3) as a product of the residual ion wave function $\Phi_{A^{2+}}$ and the two-body wave function $\Psi_{\mathbf{p}_1,\mathbf{p}_2}$ of the photo- and Auger electrons moving in the field of the A^{2+} ion. In turn the two-body wave function $\Psi_{\mathbf{p}_1,\mathbf{p}_2}$ is written as a product,

$$\Psi_{\mathbf{p}_1,\mathbf{p}_2}(\mathbf{r}_1, \mathbf{r}_2) = \Psi_{\mathbf{p}_1}(\mathbf{r}_1)\Psi_{\mathbf{p}_2}(\mathbf{r}_2)\phi(\mathbf{r}_1 - \mathbf{r}_2), \quad (4)$$

where single-particle wave functions $\Psi_{\mathbf{p}_{1,2}}(\mathbf{r}_{1,2})$ describe photoelectron and Auger electrons moving in the field of the doubly charged ion, and $\phi(\mathbf{r}_1 - \mathbf{r}_2)$ describes their relative motion.

Evaluating the PCI amplitude $\mathcal{A}$ (3), we take into account that the Auger decay operator $\hat{M}_2$ acts on the atomic and Auger electron coordinates, and does not affect directly the photoelectron coordinates. Hence, the typical values of Auger electron coordinates in the matrix element $\mathcal{A}$ are about $r_2 \sim 1$. On the other hand, integration over the photoelectron coordinates in $\mathcal{A}$ is performed on the much larger scale $r_1 \sim v_1/\Gamma \gg 1$ due to the smallness of the autoionization width Γ; v_1 is the photoelectron velocity. For 2 eV photoelectrons, this estimation gives $r_1 \sim 100$. This fact decouples the integrations over Auger electron and photoelectron coordinates, and the amplitude $\mathcal{A}$ reduces to the product of photoionization amplitude M_1, the amplitude of Auger decay M_2, and the overlapping integral:

$$\mathcal{A} = M_1\, M_2(\mathbf{p}_2, L, M)\, \langle \Psi_{\mathbf{p}_1}(\mathbf{r})\phi(\mathbf{r}) | \Psi_{\varepsilon_0+i\Gamma/2}(\mathbf{r}) \rangle. \quad (5)$$

The Auger amplitude $M_2(\mathbf{p}_2, L, M)$ depends on the quantum numbers of the residual ion A^{2+} and on the direction of the Auger emission. However, it does not affect the angular distribution of the photoelectrons if the quantum numbers of the resulting A^{2+} ion are not fixed. It can be demonstrated that during the evaluation of the cross section, after summation over all angular-momentum states M of the A^{2+} ion, the angular dependence of $|M_2(\mathbf{p}_2)|^2$ vanishes for symmetry reasons. Indeed, the Auger electron $e_A(\mathbf{p}_2)$ and the residual ion A^{2+} yield the same angular momentum L with opposite projections $\pm M$. The Auger amplitude depends on M and $\mathbf{p}_2$ as $M_2(\mathbf{p}_2, L, M) \propto Y_{LM}(\mathbf{p}_2)$. Thus, the sum of $|M_2(\mathbf{p}_2, L, M)|^2$ over M eliminates its dependence on the direction of $\mathbf{p}_2$ since $\sum_M |Y_{LM}(\mathbf{p}_2)|^2 = (2L+1)/4\pi$. Therefore, amplitudes M_2 and M_1 are considered as constant factors while the energy and angular dependencies of PCI amplitude $\mathcal{A}$ are given by the overlapping integral in Eq. (5).

The next simplification of the PCI amplitude $\mathcal{A}$ is based on the large velocity of the fast Auger electron, $v_2 \gg 1$. Since the Auger electron rapidly leaves the reaction zone with minor effect on the slow photoelectron motion, the wave function of their relative motion $\phi(\mathbf{r})$ can be treated perturbationally [25,26]. As a result, the photoionization cross section is given by a sequence of approximations [25]. In the zeroth approximation, neglecting the direct interaction between photoelectrons and Auger electrons, $\phi(\mathbf{r}) = 1$ and the cross section is given by

$$\frac{d^2\sigma^{(0)}}{d\varepsilon\, d\Omega} = \frac{M}{4\pi} |R_{\varepsilon\, 1,\varepsilon_0\, 1}|^2 [1 + 2P_2(\cos\theta)], \quad (6)$$

where M is the numerical factor containing the product of the photon absorption cross section and the Auger decay cross section that depends smoothly on ε; $R_{\varepsilon\, l,\varepsilon_0\, 1}$ is the overlapping integral between the radial parts $\chi(r)$ of the photoelectron wave functions in the intermediate, $\varepsilon = \varepsilon_0 + i\Gamma/2$, $l = 1$, and final, $\varepsilon = p_1^2/2$, $l = 1$, electron states:

$$R_{\varepsilon\, l,\varepsilon_0\, 1} = \int_0^\infty \chi_{\varepsilon,\, l}(r)\chi_{\varepsilon_0 + i\frac{\Gamma}{2},\, 1}(r)dr. \quad (7)$$

The photoelectron in the intermediate state, prior to Auger decay, propagates in the field of the singly charged ion with the complex energy $\varepsilon_0 + i\frac{\Gamma}{2}$. In the final state, after the Auger decay, the photoelectron with energy ε propagates in the field on the doubly charged ion. Both wave functions are obtained numerically in the framework of the Hartree-Fock approximation. The diverging wave function $\chi_{\varepsilon_0+i\frac{\Gamma}{2},\, 1}(r)$ is obtained as a solution of the inhomogeneous Schrödinger equation

with complex energy $\varepsilon_0 + i\Gamma/2$ by the method described in [16,17]. According to Eq. (6) the zero approximation neglects the angular-momentum transfer, the photoelectron angular momentum in the final state is the same as in the intermediate state $l = 1$. The distortion of the cross section energy profile given in Eq. (6) by the overlapping integral $R_{\varepsilon\,1,\varepsilon_0\,1}$ is caused by interaction of the photoelectron with the ionic field that undergoes a sudden change due to the Auger decay [16].

The angular-momentum transfer between photoelectron and Auger electron is taken into account in the next approximation by means of the first Born approximation. The corresponding cross section is equal to (see Refs. [25,26] for the details)

$$\frac{d^2\sigma^{(2)}}{d\varepsilon\, d\Omega} = \frac{3M}{4\pi}\left(\frac{e^2}{v}\right)^2 \sum_k P_k(\cos(\theta)) C^{k0}_{10\,10} \sum_{l_1,l_2,l>0} e^{i(\delta_{l_1}-\delta_{l_2})} i^{l_2-l_1}(-1)^{l+l_1+l_2} R_{\varepsilon\,l_1,\varepsilon_0\,1} R^*_{\varepsilon\,l_2,\varepsilon_0\,1} \frac{(2l+1)}{l^2(l+1)^2}$$
$$\times\sqrt{(2l_1+1)(2l_2+1)} \begin{Bmatrix} l & l_2 & 1 \\ k & 1 & l_1 \end{Bmatrix} C^{k0}_{l_1 0\, l_2 0} C^{l_1 0}_{l0\,10} C^{l_2 0}_{l0\,10}. \quad (8)$$

Here, $C^{k0}_{l_1 0\, l_2 0}$ are the Clebsch-Gordan coefficients, factor M has the same value as in Eq. (6), $v = v_2 - v_1$, v_2 is the velocity of the Auger electron, v_1 is the velocity of the photoelectron, the overlapping integrals $R_{\varepsilon\, l,\varepsilon_0\, 1}$ are defined by expression (7), and δ_l are the phases of the outgoing photoelectron wave functions. Note that overlapping integrals $R_{\varepsilon\, l,\varepsilon_0\, 1}$ include the photoelectron final state wave functions $\chi(r)$ with different angular momenta $l \neq 1$; it means that different angular momenta l can be transferred to the photoelectron.

Equations (6) and (8) give the cross sections of the photoionization processes with fixed electron configuration and the L term of the residual doubly charged ion. This selectivity is contained in the constant factor M. If the final state of the A^{2+} ion is not selected experimentally, as it takes place under

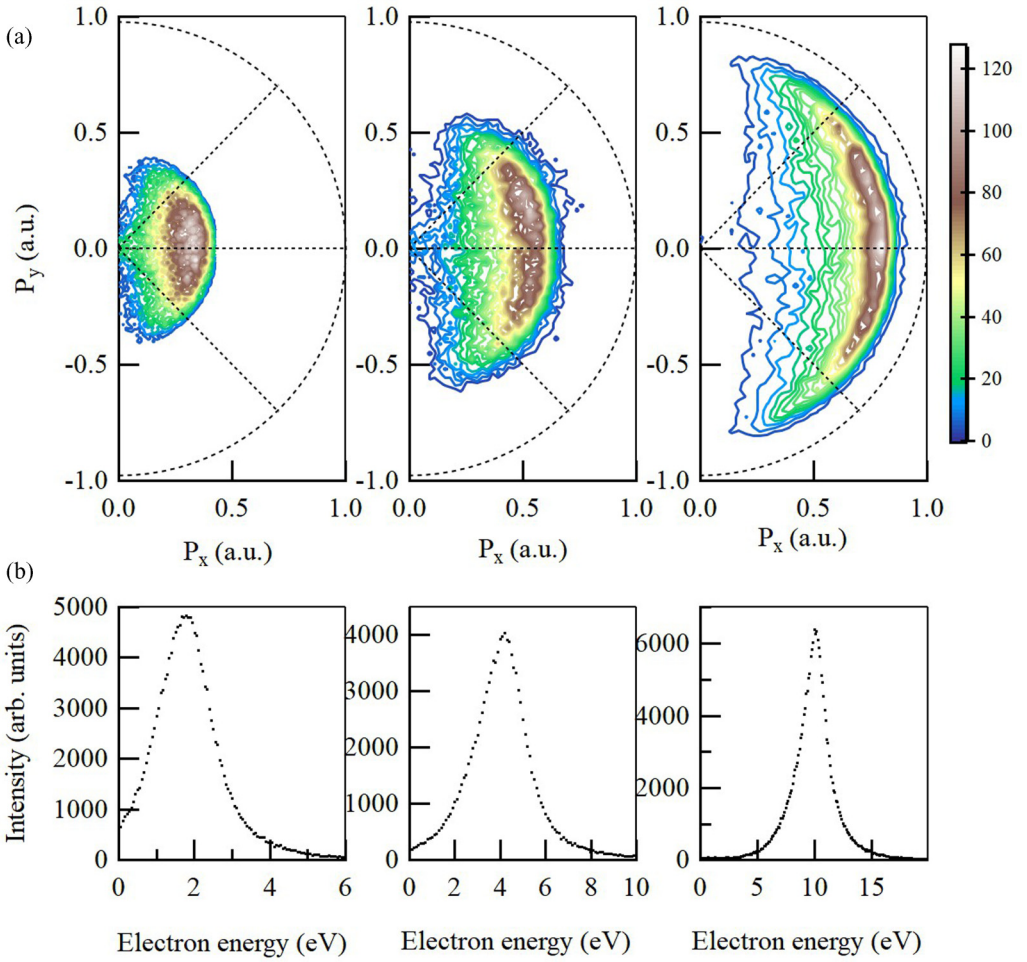

FIG. 2. (a) Projections of the P_x and P_y components of the photoelectron momentum. Left, at 2 eV of excess photon energy above threshold; center, at 4 eV of excess energy; right, at 10 eV of excess energy. Only the positive half of the projection along the x axis is shown to reduce the size of the figure. The negative half is simply the symmetrical image. (b) Corresponding kinetic energy distributions.

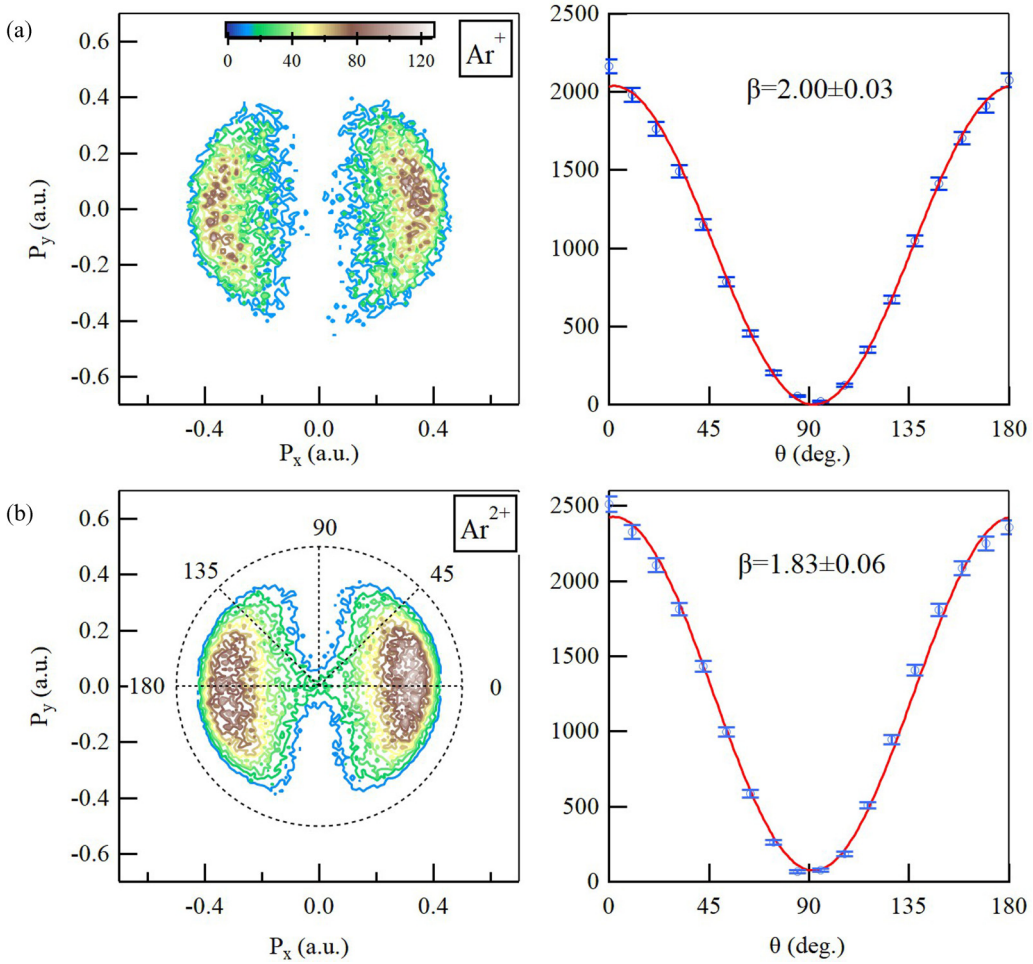

FIG. 3. (a) Photoelectron angular distribution measured in coincidence with the singly- charged Ar^+ ion for excess photon energy $\Delta E = 2$ eV. Left: projection of the P_x and P_y components of the momentum. Right: number of counts as a function of the emission angle with respect to the polarization vector, and fit using the well-known dipole angular distribution formula (see text). (b) The same for photoelectrons measured in coincidence with the doubly charged Ar^{2+} ion.

our experimental conditions, the total cross section is given by a sum of cross sections with different final states of residual ions.

Note that the different terms of the same electron configuration as well as the fine structure splitting lead to the final states of the A^{2+} ion with close energies. Hence, the corresponding Auger electron energies are also close and the photoelectron overlapping integrals show very similar behavior. Therefore, an account of different Auger transitions in this case changes the value of the factor M uniformly in the cross sections (6) and (8) and does not change the β value.

The decay of the inner $1s$ vacancy shows a rather complicated dynamics [1]. We are interested in the PCI process resulting in Ar^{2+} ions via Auger decay. The main channel leading to the creation of the Ar^{2+} ions includes the radiative decay of the inner vacancy $1s^{-1} \to 2p^{-1} + \gamma$ followed by the Auger decay $2p^{-1} \to 3p^{-2} + e_A$ with emission of fast Auger electron e_A ($E_A \simeq 200$ eV) [27]. The widths of the $1s$ and $2p$ vacancies are equal to $\Gamma_{1s} = 690$ meV and $\Gamma_{2p} = 118$ meV [1], respectively. The first radiative decay $1s^{-1} \to 2p^{-1} + \gamma$ of the inner vacancy occurs after long delay $\tau_{1s} = 1/\Gamma_{1s}$ when the photoelectron has already moved away from the ion. Although the radiative decay gives rise to some asymmetry of the ionic field, its influence on outgoing photoelectrons is too weak to explain the observed angular distribution distortion because of the large distance between Ar^{+*} and e_{ph} [25] and can be therefore neglected. The considerable impact on the outgoing electron motion, the shake-off, takes place only at the moment of the Auger decay. Again, as shown in [25], the asymmetrical part of the interaction between photoelectron and the residual ion Ar^{2+} could not provide sizable angular-momentum transfer due to the large interparticle distance. The main contribution to the angular-momentum transfer comes from interaction between photo- and Auger electrons. That is why in describing this process we can treat for simplicity the two-step decay process as a single Auger decay with the effective decay time $\tau_{\text{eff}} = \tau_{1s} + \tau_{2p}$ and corresponding effective autoionization width $\Gamma_{\text{eff}} = \Gamma_{1s}\,\Gamma_{2p}/(\Gamma_{1s} + \Gamma_{2p})$ [1,25]. In our case, it gives $\Gamma_{\text{eff}} = 101$ meV.

This channel is in competition with various weaker decay channels, e.g., the direct Auger decay of the inner $1s$ vacancy $1s^{-1} \to 3p^{-2} + e_A$ with the Auger electron energy $E_A \simeq 3150$ eV [27]. Also, the Auger decay of the vacancy $2p^{-1}$ in Ar^{+*}, resulting from the radiative decay of the inner

shell vacancy $1s^{-1}$, can lead to other final electron configurations of the Ar^{2+} ion, namely $3s^{-1}3p^{-1}$ and $3s^{-2}$. Each channel gives independent contributions to the ionization cross section according to Eqs. (6) and (8). However, the intensities of the competitive Auger processes are too small [27] to distort the photoemission angular distribution. In the case of direct Auger decay, there is an additional reason why its contribution to the asymmetry parameter is negligible. An Auger electron resulting from direct Auger decay is much faster than an Auger electron emitted in a cascade process; its energy is $E_A \simeq 3150$ eV compared to $E_A \simeq 200$ eV in the cascade decay [27]. According to Eq. (8), the efficiency of angular-momentum exchange between the photoelectron and the Auger electron is inverse to the square of their relative velocity v. That is why, evaluating the asymmetry parameter β, we restrict ourselves to the main decay process (2).

III. RESULTS AND DISCUSSION

In Fig. 2, top, we show projections of the P_x and P_y components of the photoelectron momentum, measured at three different values of excess energy above threshold (2, 4, and 10 eV). Only the positive half of the projection along the x axis is shown to reduce the size of the figure. The negative half is simply the symmetrical image. In Fig. 2, bottom, we show the corresponding kinetic energy distributions. The kinetic energy distribution clearly shows the distortion from a symmetrical line shape and a shift in the maximum of distribution due to PCI at low excess photon energy above threshold, in agreement with the observations made previously [1]. PCI distortion of the photoelectron energy distribution is stronger at 2 eV above threshold, moderate at 4 eV above threshold, and becomes negligible within our experimental resolution at 10 eV above threshold. This observation illustrates the photon energy dependence of PCI.

In Fig. 3, we show photoelectron angular distribution obtained for photoelectrons of 2 eV kinetic energy in coincidence with the Ar^+ ion (top) and the Ar^{2+} ion (bottom). The horizontal axis coincides with the direction of the synchrotron radiation polarization vector. In the left side of both panels, projection of the P_x and P_y components of the momentum are shown, and in the right side are numbers of counts as a function of the emission angle with respect to the polarization vector, fit using the well-known angular distribution formula (see above). A significant difference is evident even by eyesight. In particular, while for photoelectron emission in coincidence with Ar^+ the distribution reflects the expected $P_2(\cos\theta)$ one, for the Ar^{2+} pattern a deviation from it is rather clear.

In Fig. 4, top, the experimental β angular distribution parameter is shown for three values of photoelectron kinetic energy, 2, 4, and 10 eV, in coincidence with either Ar^+ or Ar^{2+}. The experimental data show a β value equal to 2 for all kinetic energies measured in Ar^+-photoelectron coincidences. This result can be immediately interpreted on the ground of this consideration: for singly charged Ar ions, there is no Auger electron emission, and therefore no perturbation on the photoelectron pathway.

For the Ar^{2+}-photoelectron coincidence measurements, the situation is clearly different: a significant deviation from the

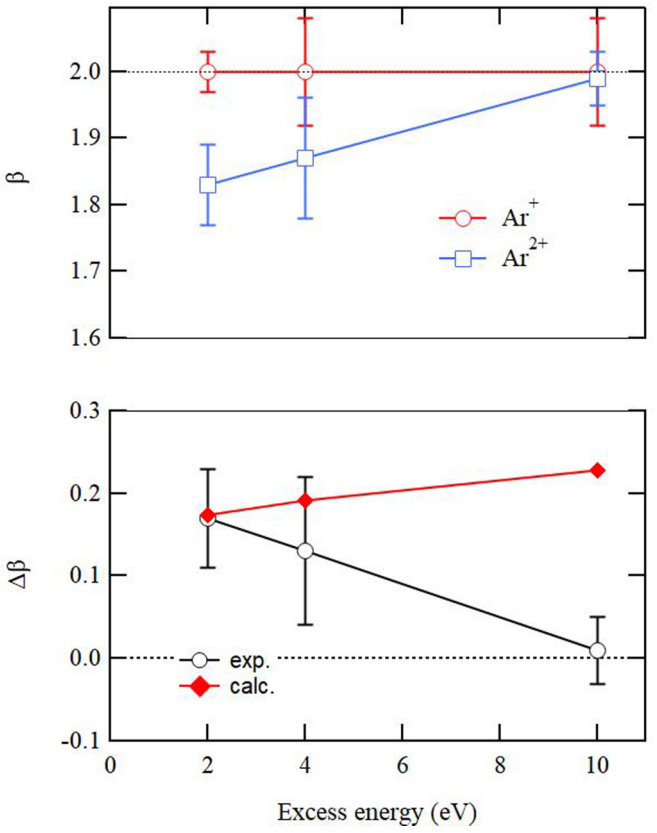

FIG. 4. Top: measured β values for photoelectrons in coincidence with Ar^+ and Ar^{2+} at 2, 4, and 10 eV of excess photon energy. Bottom: experimental and calculated values for $\Delta\beta$, the deviation of β from 2, as a function of excess energy.

$\beta = 2$ expected value is observed, which can be attributed to a photoelectron–Auger-electron exchange of some kind. Fig. 4, bottom, shows the experimental and calculated deviation of β from 2, $\Delta\beta = 2 - \beta$.

Our calculations of the asymmetry parameter β, averaged over the line profile, give the following values for the deviation: $\Delta\beta = 0.174$ for excess energy $\Delta E = 2$ eV, $\Delta\beta = 0.191$ for $\Delta E = 4$ eV, and $\Delta\beta = 0.228$ at 10 eV excess energy. The agreement with the experimental data is satisfying within statistical error at low excess energy, where the experimental values are found to be $\Delta\beta = 0.17 \pm 0.06$ at 2 eV and $\Delta\beta = 0.13 \pm 0.09$ at 4 eV. However, experimental data and calculated values are in disagreement at 10 eV excess energy, where the experiment shows $\Delta\beta = 0.01 \pm 0.04$. Moreover, the general trend as a function of excess energy is opposite, $\Delta\beta$ rapidly decreasing to 0 in the experiment, while it keeps going up in the theory [26]. This behavior found in the calculation results is connected with the decrease of relative electron velocity v under the increase of the photon excess energy that makes interaction between the Auger electron and the photoelectron more effective.

IV. CONCLUSION

We demonstrate here that in core-ionized argon the "standard" PCI model taking into account only photoelectron–residual-ion interaction is not sufficient to describe the details of photoelectron emission. Therefore, we have extended it to

include not only energy exchange but also angular-momentum exchange between the photoelectron and the Auger electron. On the grounds of our new experimental results and of the developed theoretical model, the effective existence and main mechanism of angular-momentum transfer due to PCI in deep inner-shell ionization and its effect on the asymmetry parameter β near the photoionization threshold are therefore illuminated. The discrepancy between theoretical and experimental trends concerning the strength of the effect will be the subject of further investigations.

[1] R. Guillemin, S. Sheinerman, C. Bomme, L. Journel, T. Marin, T. Marchenko, R. K. Kushawaha, N. Trcera, M. N. Piancastelli, and M. Simon, Phys. Rev. Lett. **109**, 013001 (2012).

[2] M. Simon, R. Püttner, T. Marchenko, R. Guillemin, R. K. Kushawaha, L. Journel, G. Goldsztejn, M. N. Piancastelli, J. M. Ablett, J.-P. Rueff, and D. Céolin, Nat. Commun. **5**, 4069 (2014).

[3] R. Guillemin, P. Decleva, M. Stener, C. Bomme, T. Marin, L. Journel, T. Marchenko, R. K. Kushawaha, K. Jänkälä, N. Trcera, K. P. Bowen, D. W. Lindle, M. N. Piancastelli, and M. Simon, Nat. Commun. **6**, 6166 (2015).

[4] R. Guillemin, S. Sheinerman, R. Püttner, T. Marchenko, G. Goldsztejn, L. Journel, R. K. Kushawaha, D. Céolin, M. N. Piancastelli, and M. Simon, Phys. Rev. A **92**, 012503 (2015).

[5] R. Guillemin, K. Jänkälä, B. C. de Miranda, T. Marin, L. Journel, T. Marchenko, O. Travnikova, G. Goldsztejn, I. Ismail, R. Püttner, D. Céolin, B. Lassalle-Kaiser, M. N. Piancastelli, and M. Simon, Phys. Rev. A **97**, 013418 (2018).

[6] M. Yu. Kuchiev and S. A. Sheinerman, Sov. Phys. Usp. **32**, 569 (1989).

[7] V. Schmidt, Rep. Prog. Phys. **55**, 1483 (1992).

[8] A. K. Kazansky and N. M. Kabachnik, Phys. Rev. A **72**, 052714 (2005).

[9] F. Penent, S. Sheinerman, L. Andric, P. Lablanquie, J. Palaudoux, U. Becker, M. Braune, J. Viefhaus, and J. H. D. Eland, J. Phys. B **41**, 045002 (2008).

[10] L. Gerchikov and S. Sheinerman, Phys. Rev. A **84**, 022503 (2011).

[11] S. Sheinerman, P. Linusson, J. H. D. Eland, L. Hedin, E. Andersson, J. E. Rubensson, L. Karlsson, and R. Feifel, Phys. Rev. A **86**, 022515 (2012).

[12] J. Palaudoux, S. Sheinerman, J. Soronen, S.-M. Huttula, M. Huttula, K. Jänkälä, L. Andric, K. Ito, P. Lablanquie, F. Penent, J.-M. Bizau, S. Guilbaud, and D. Cubaynes, Phys. Rev. A **92**, 012510 (2015).

[13] M. Ya. Amusia, M. Yu. Kuchiev, and S. A. Sheinerman, Sov. Phys. JETP **49**, 238 (1979).

[14] K. Helenelund, S. Hedman, L. Asplund, U. Gelius, and K. Siegbahn, Phys. Scr. **27**, 245 (1983).

[15] G. B. Armen, T. Aberg, J. C. Levin, B. Crasemann, M. H. Chen, G. E. Ice, and G. S. Brown, Phys. Rev. Lett. **54**, 1142 (1985).

[16] M. Yu. Kuchiev and S. A. Sheinerman, J. Phys. B **18**, L551 (1985).

[17] M. Yu. Kuchiev and S. A. Sheinerman, Comput. Phys. Commun. **39**, 155 (1986).

[18] D. Dill, A. F. Starace, and S. T. Manson, Phys. Rev. A **11**, 1596 (1975).

[19] S. T. Manson and A. F. Starace, Rev. Mod. Phys. **54**, 389 (1982).

[20] R. Guillemin, C. Bomme, T. Marin, L. Journel, T. Marchenko, R. K. Kushawaha, N. Trcera, M. N. Piancastelli, and M. Simon, Phys. Rev. A **84**, 063425 (2011).

[21] L. Journel, R. Guillemin, A. Haouas, P. Lablanquie, F. Penent, J. Palaudoux, L. Andric, M. Simon, D. Céolin, T. Kaneyasu, J. Viefhaus, M. Braune, W. B. Li, C. Elkharrat, F. Catoire, J.-C. Houver, and D. Dowek, Phys. Rev. A **77**, 042710 (2008).

[22] C. Bomme, R. Guillemin, T. Marin, L. Journel, T. Marchenko, D. Dowek, N. Trcera, B. Pilette, A. Avila, H. Ringuenet, R. K. Kushawaha, and M. Simon, Rev. Sci. Instrum. **84**, 103104 (2013).

[23] D. Vantelon, N. Trcera, D. Roy, T. Moreno, D. Mailly, S. Guilet, E. Metchalkov, F. Delmotte, B. Lassalle, P. Lagarde, and A.-M. Flank, J. Synchrotron Radiat. **23**, 635 (2016).

[24] K. Ueda, E. Shigemasa, Y. Sato, A. Yagishita, M. Ukai, H. Maezawa, T. Hayaishi, and T. Sasaki, J. Phys. B **24**, 605 (1991).

[25] L. Gerchikov, R. Guillemin, M. Simon, and S. Sheinerman, Phys. Rev. A **95**, 063425 (2017).

[26] L. Gerchikov and S. Sheinerman, J. Phys. B **51**, 065201 (2018).

[27] U. Alkemper, J. Doppelfeld, and F. von Busch, Phys. Rev. A **56**, 2741 (1997).